ISSN 1946-7664. MCFNS 2020
Vol. 12, Issue 1, pp. 16–25
Mathematical and Computational Forestry & Natural-Resource Sciences

AVAILABLE ONLINE AT HTTP://MCFNS.COM

Submitted: Mar. 11, 2019
Accepted: Dec. 5, 2019
Published: Mar. 30, 2020
Last Correction: Mar. 30, 2020

AN OPTIMIZED MODEL FOR PREDICTING FOREST FIRES AREA BASED ON BINOCULAR VISION

Xingdong Li[1,3], H. Gao[1], C. Han[1], Y. Wang[1], T. Hu[2,3], L. Sun[2,3*], Y. Guo[1*]

[1] *College of Mechanical and Electrical Engineering, Northeast Forestry University, Harbin 150040, China;*

[2] *College of Forestry, Northeast Forestry University, Harbin 150040, China;*

[3] *Northern Forest Fire Management Key Laboratory of the State Forestry and Grassland Bureau, Northeast Forestry University, Harbin 150040, China*

Abstract. Forecasting of forest fire area is of great significance to effectively control the spread of forest fire. In this paper, the forest fire spreading velocity model and the forest fire spreading simulation technology based on huygens principle are used to estimate the forest fire area. Firstly, binocular camera is used to collect the firing state data of wild forest fire, and segment the firing image, extract the firing line, locate the firing line and calculate the three-dimensional coordinates of the firing line pixels according to perspective projection model. Secondly, the forest fire spreading velocity model based on Wang Zhengfei's model is redesigned. The model parameters of forest fire area were optimized by gradient method. The prediction accuracy is much higher than that of the model before optimization.

Keywords: Forest fire area prediction; Wang Zhengfei's model; Huygens principle; binocular camera; image segmentation; regression analysis

1 Background

The frequent occurrence of forest fires has attracted great attention in recent years. Last November, a fire in California destroyed more than 19,000 buildings, killed about 85 people, damaged more than 60,000 hectares and burned the small town of paradise to the ground; In August this year, an even more shocking fire broke out in the amazon rainforest. As of this writing, the number of amazon forest ignition points reached 75,336, and the fire area has exceeded 800,000 hectares. How to better understand the fire, predict the fire, prevent and control the fire has become an increasingly urgent problem.

Since the beginning of the 20th century, researchers in different disciplines (e.g., Milios et al. 2018, Willson et al. 2019) have carried out various projects to study the main factors affecting forest fire behavior. Based on the statistical analysis of a large number of observations and experimental data, a forest fire spreading model was established based on the physical processes of chemical change and heat transfer of forest fire combustion. In recent years, due to the rapid development of computer technology, the forest fire spread modeling has advanced to computationally intensive spatial simulation modeling (Wang et al., 2013). Because of the complexity of forest fire spread and the influence of many factors, it is very important to us the video image to monitor the forest fire for extracting forest fire characteristics and predicting its spread. Based on image vision, Han (2017) used the background subtraction motion detection method based on gaussian mixture model to extract the moving target from the video stream, and combined with the multi-color detection of RGB, HSI and YUV color space to obtain the possible fire area, the proposed method can achieve better effectiveness, adaptability and robustness; Wu (2015) proposed an algorithm for flame detection based on fusion of circularity, rectangularity and the coefficient of orthocenter height and input these features into SVM for classification. The proposed algorithm is efficient and fast for fire detection, and it could detect fire real-time under a variety of circumstances. Through the processing of video images, real-time forest fire spread data can be acquired effectively. Through the analysis of experimental data and the selection of appropriate data processing means, an effective forest fire spread model can be established. Yang (2016) used Unity to build three-dimensional terrain and improved cellular automata to simulate the spread of forest fires. He modeled and simulated three different terrain vegetation respectively; Tang (2015) developed a three-

dimensional visual simulation system based on the FARSITE forest fire spreading simulation engine, which can simulate the forest fire spreading process under the influence of different combustible substances, topography and meteorological factors, predict forest fire behaviors and evaluate fire occurrence areas.

As shown in Fig. 1, the first part of the paper introduces how to preprocess the image collected by binocular camera and extract the fire line at each time, and convert it into actual coordinate system through a PCL point cloud. The second part establishes the forest fire area spread model by using the revised Wang Zhengfei's model and Huygens principle. In the third part, the optimization objectives of the spread model parameters are defined according to the experimental data, and establish the gradient descent mathematical model. The vertical and horizontal evaluation of the optimized forest fire area spread model is carried out from two aspects of goodness of fit and residuals.

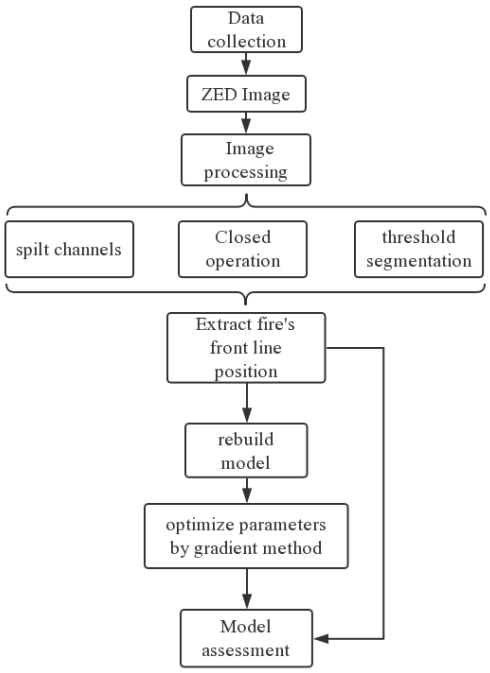

Figure 1: system flowchart

2 Binocular image preprocessing

In the traditional forest fire experiment or on-the-spot survey, most of the experiment data collected from the forest fire are carried out artificially. For example, in order to collect the spread rate of fire, it is necessary to lay thermocouples in advance in the experimental fire field, and to estimate the spread rate of fire through temperature sensing, which is very time-consuming and consumes a lot of manpower and material resources. ZED binocular stereo camera (Wang et al., 2019) is used to collect the relevant data of the fire field. Through the built-in API of ZED camera, the pixel distance can be easily transferred to the real three-dimensional distance, and the data acquisition efficiency is very efficient.

2.1 DH parameters of the model

Binocular localization is a commonly used method in three-dimensional reconstruction. Depth information can be obtained by geometric constraints using parallax between images captured by two cameras. In normal three-dimensional reconstruction, the texture of the object surface has a great impact on the reconstruction effect, so it is necessary to take multi-angle photographs of the same object to get a better three-dimensional reconstruction model. However, the forest fire spread model in the paper, we only need to collect the speed of fire spread, so it is not very related to the shape of the fire itself. ZED camera can be set up to take pictures at fixed points at fixed points, so as to capture the spread trend of fire, and the spread speed at actual distance can be obtained by coordinate transformation.

Binocular localization uses two cameras to take pictures, and uses least square method to realize three-dimensional reconstruction (Technikova et al., 2016). A simple model of binocular positioning is shown in Fig. 2.

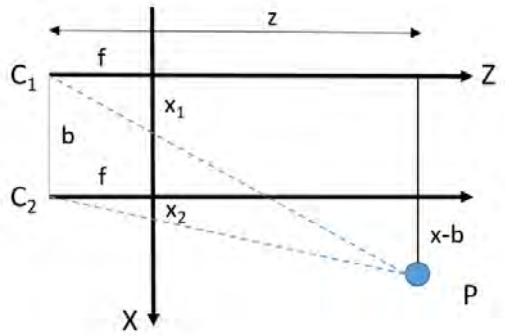

Figure 2: The model of Binocular Location

Assuming that the object and the two cameras in the space are arranged in the relationship show above, $C1$ and $C2$ are two identical cameras, whose internal and external parameters can be obtained by Zhang Youzheng camera calibration method (Zhao et al., 2018), and f is the camera focal length obtained by calibration. Let $C1$

coordinate system be $O1x1y1z2$, $C2$ coordinate system be $O2x2y2z2$, and the distance between two cameras is B. The coordinates of any point P in space (x, y, z) and the axis y are perpendicular to the paper surface. According to the triangle similarity relation, the following relations can be obtained as the Eq. (1).

$$\begin{cases} \frac{z}{f} = \frac{x}{x_1} \\ \frac{z}{f} = \frac{x-b}{x_2} \\ \frac{z}{f} = \frac{y}{y_1} = \frac{y}{y_2} \end{cases} \tag{1}$$

According to the Eq. (1), infer the depth z of point P as the Eq. (2):

$$z = \frac{f \cdot b}{x_1 - x_2} = \frac{f \cdot b}{d} \tag{2}$$

From Eq. (1) and Eq. (1), we can deduce the x and y values of space point P as the Eq. (3):

$$\begin{cases} x = \frac{x_1 \cdot z}{f} \\ y = \frac{y_1 \cdot z}{f} \end{cases} \tag{3}$$

The three-dimensional coordinates of any point in the image can be obtained efficiently by using Zhang Zhengyou's camera calibration method (Liu et al., 2017) and binocular positioning. This method is very helpful for collecting forest fire spread data. The depth map can be obtained by ZED camera as shown in Fig. 3.

(a) Ordinary image (b) Depth image

Figure 3: RGB image and depth image

2.2 Image Segmentation

After ZED image acquisition, in order to obtain the coordinate of the fire front at every moment, image augmentation is needed to extract the fire from the whole picture.

2.2.1 Color space preprocessing

A common color space in computer is RGB color space, which is based on three basic colors: R (Red), G (Green), B (Blue) to produce rich and extensive colors. However, as can be seen from Fig. 3, the color of fire is not every different from that of surrounding brown meadows, so this color space can bot accurately extract the color features of fire. Considering the heat and luminescence of the fire itself, the difference between the fire and the surrounding scenery is mainly due to the different brightness. The brightness of the fire should be much higher than that of the surrounding scenery. Therefore, image preprocessing is based on YCrCb color space (Al-Tairi et al., 2014), which reflects brightness information. YCrCb color space describes color by the relationship between brightness and color difference. Y channel describes brightness, and both Cr and Cb are chroma channels. The original image of Fig. 3 is separated by channels, as shown in Fig. 4.

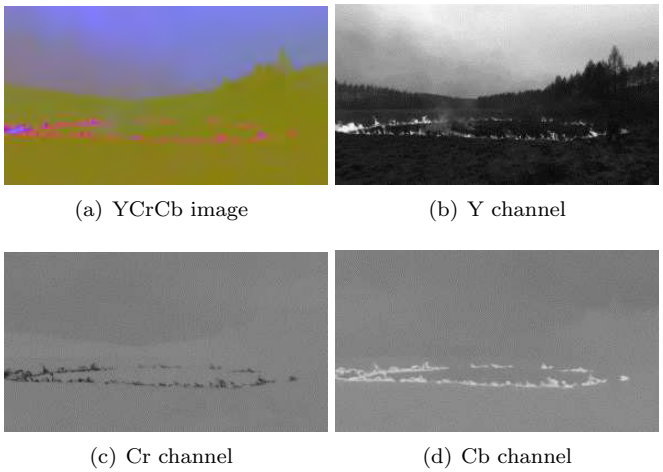

(a) YCrCb image (b) Y channel

(c) Cr channel (d) Cb channel

Figure 4: YCrCb Image Channel Separation

As can be seen from Fig. 4, the YCrCb color space with brightness information considerations can extract fire color features well. There is a great difference between the fire pixel value in the Cr channel and the surrounding scenery, so this paper chooses the Cr channel as the object of further processing. In order to enhance the characteristics of fire, image closed operation is performed on Cr channel. Closed operation is an operation that expands the image first and then corrodes it. It is used to remove small noise points and to connect the fire wires to a certain extent, as shown in Fig. 5.

For the image after closed operation, the fire line and the surrounding scenery have obvious differences, and then binary threshold segmentation can separate the fire from the whole picture, as shown in Fig. 6.

2.2.2 Data Extraction

In the above, the processing of a single picture is completed. In the whole video, the video image after image

Figure 5: Closed operation of image

Figure 6: Binary threshold segmentation

preprocessing can be obtained by processing the continuous frames. The fire image reflected by each picture is only the spread change under the pixel distance, and the fire area corresponding to each picture can be converted into the fire area in the real space by PCL of point cloud. In this paper, a total of about 2 minutes of video was recorded. 64 frames were randomly selected as data processing frames. The first 50 frames were used as training data to optimize the model, and the last 14 frames were used to evaluate the regression model.

3 Establishment of forest fire spreading model

3.1 Forest Fire Spread Velocity Model

At present, the main models of forest fire spread in the world are Rothermel model in the United States (Ervilha et al., 2017), MacArthur model in Australia (Wang et al., 2013), Canadian forest fire spread model (Wang et al., 2013), Wang Zhengfei spread model in China (Wang et al., 2013), and various modified models evolved on the basis of these models. Based on the comprehensive consideration of various environmental conditions and experimental equipment, Wang Zhengfei's model is selected as the deduction formula of speed, and the improved analysis of forest fire spread model is carried out by combining Huygens'principle.

Wang Zhengfei's model is based on a large number of spot burning experiments. According to the temperature, humidity and wind level of the fire field, an initial spreading velocity R_0 is given, and then a constant coefficient is given according to the terrain, wind speed and types of combustibles. Finally, the formula of forest fire spreading speed is obtained as Eq. (4).

$$\begin{cases} R_0 = a \cdot T + b \cdot V + c \cdot h - d \\ R = R_0 \cdot K_s \cdot K_\phi \cdot K_f \end{cases} \tag{4}$$

In the formula: R_0 is the initial forest fire spreading speed (m/min); a, b, c, d constant; T is the temperature (°C), V is the Buffalo wind level, h is the air humidity(%); R is the forest fire spreading speed (m/min); K_s, K_ϕ, K_f are the combustible index, wind coefficient and topographic coefficient respectively the three coefficients can be obtained through a look-up table (Chen et al., 2012).

In this paper, meadow site is chosen as the burning site, and there is not too much slope fluctuation, so the topographic coefficient K_f and wind speed coefficient K_ϕ are not considered for the time being, because in Huygens Principle, the influence of various directions of fire spread will be taken into account, and the consideration of wind speed coefficient will be discussed below. In order to better simulate the trend of forest fire spread, four constants (a, b, c, d) and combustible index K_s in the initial forest fire spread rate R_0 are modified. Because the exponents of Wang Zhengfei's model are derived from a large number of experiments, the revision of Ks only fluctuates in a small range. The modified KS is given by Eq. (5).

$$KS = K_s^{\frac{10}{10+\sin e}} \tag{5}$$

In the formula: KS is a new parameter after modification, and finally the forest fire spreading speed R is obtained as Eq. (6):

$$R = R_0 \cdot KS \cdot K_\phi \cdot K_f = R_0 \cdot K_s^{\frac{10}{10+\sin e}} \tag{6}$$

3.2 Forest Fire Area Spread Simulation Based on Huygens Principle

Although Wang Zhengfei's model can accurately estimate the spreading speed of forest fires at a certain time, it is not accurate enough to describe the spreading area of forest fires and the speed of each direction of fire spread. In this paper, the data obtained from ZED image processing are mostly the area of fire field at each time, so in order to better describe the experimental data entering Huygens principle. Huygens principle explains the propagation of elliptical expansion in the front propagation of light wave, which Richards (Richards and Gwynfor, 1994) applied to wild-fires.

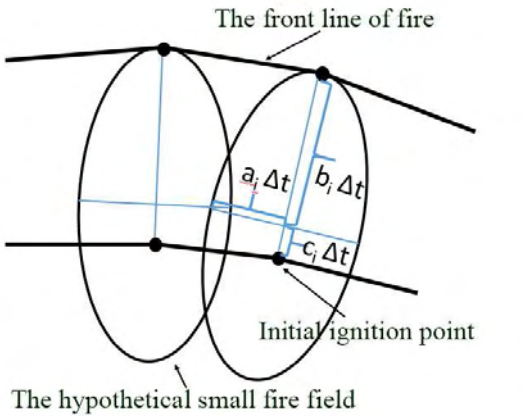

Figure 7: Forest Fire Spread Based on Huygens Principle

As shown in Fig. 7, assuming that every point around the fire field is a new fire point and propagates within a unit time t, an elliptical small fire field is formed. Let the coefficient LB be the ratio of length to width of elliptical small fire field, which is related to the wind speed (H. E, 1983).

$$\begin{cases} LB(t) = \\ 0.936^{0.2566U(t)} + 0.461^{-0.1548U(t)} - 0.397 \\ HB = \dfrac{LB + \sqrt{LB^2 - 1}}{LB - \sqrt{LB^2 - 1}} \end{cases} \tag{7}$$

$U(t)$ is the wind speed. In the small elliptical fire field, a is the lateral velocity, $(b+c)$ is the front and the outside velocity. Based on Wang Zhengfei's model and geometric relation, a, b and c can be obtained as shown in Eq. (8).

$$\begin{cases} a = R \cdot \dfrac{1 + a/LB}{2LB} \\ b = R \cdot \dfrac{1 + 1/HB}{2} \\ c = b - \dfrac{R}{HB} \end{cases} \tag{8}$$

If all points in the fire field are taken into account, the area of the outer circle formed by all ellipses is the area where the fire field diffuses at a certain time. According to the partial differential equation derived by Richards, the phase strain change of the fire diffusion vector can be obtained, as shown in Eq. (9).

$$\begin{cases} \Delta X(x_s, y_s) = \dfrac{\partial x(s,t)}{\partial t} = \\ \dfrac{a^2 \cos\theta(x_s \sin\theta + y_s \cos\theta) - b^2 \sin\theta(x_s \cos\theta - y_s \sin\theta)}{\sqrt{(b^2(x_s \cos\theta - y_s \sin\theta))^2 + (a^2(x_s \sin\theta + y_s \cos\theta))^2}} \\ + c \sin\theta \\ \Delta Y(x_s, y_s) = \dfrac{\partial y(s,t)}{\partial t} = \\ \dfrac{-a^2 \sin\theta(x_s \sin\theta + y_s \cos\theta) - b^2 \cos\theta(x_s \cos\theta - y_s \sin\theta)}{\sqrt{(b^2(x_s \cos\theta - y_s \sin\theta))^2 + (a^2(x_s \sin\theta + y_s \cos\theta))^2}} \\ + c \cos\theta \end{cases} \tag{9}$$

In Eq. (9), θ is the composite angle of wind direction and slope direction. In this experiment, the slope angle is not considered because the slope fluctuation is not large; t is the time of propagation and spread; x_s and y_s are the coordinates of the ignition point. According to the fitting ellipse of the fire field, the fire area at t moment can be obtained as Eq. (10).

$$S(t) = \frac{1}{4}\pi \cdot (X_0 + t \cdot \Delta X) \cdot (Y_0 + t \cdot \Delta Y) \tag{10}$$

4 Parameter optimization and evaluation of forest fire area spread model

4.1 Parameter optimization of spread velocity model

Because the area of forest fire spread is approximately linear with time, the first 50 experimental data values are optimized in MATLAB. In order to find the optimal point efficiently, the gradient descent method is used to solve the parameters of the forest fire spread model. Define the cost function as Eq. (11).

$$J(\theta) = \frac{1}{2n} \sum_{i=1}^{n} (h_\theta(x^i) - Y^i)^2 \tag{11}$$

The cost function of mean square error is chosen here, in which n is the number of data sets; 1/2 is the quadratic coefficient of a constant in order to offset the differential, which will not produce redundant constant coefficients for subsequent calculation; Y^i is the measured value of forest fire spread area corresponding to each time point in the data set. h_θ is a predictive function, i.e. the formula of forest fire spread deduced above. According to the time point x^i of each input, the predicted h_θ value is calculated. The variable h_θ is revised according to the difference between the predicted value and the measured value, and the optimal point is found through many iterations. In this paper, there are five variables: temperature coefficient a, wind level coefficient b, humidity coefficient c, constant coefficient d and combustible index coefficient e. The prediction function is as Eq. (12).

$$h_\theta(x^{(i)}) = (x^{(i)}, aT, bV, ch, d, \sin e) \tag{12}$$

From the cost function, we can see that the problem is actually solved by gradient descent of five variables. Wherein, $\sin e$ is a modified parameter of wind speed KS, which can be regarded as a constant parameter in the model operation and has no influence on the change of x. Parameters a, b, c and d constitute parameters R_0 as a superimposed system. Since KS is a constant, the change of velocity in the above-mentioned spreading

model is affected by only one parameter R_0, so this system is a linear model. The gradient of the cost function is solved by differentiating each variable separately as Eq. (13).

$$\begin{cases} \bigtriangledown J(\theta) = \langle \dfrac{\partial J}{\partial a}, \dfrac{\partial J}{\partial b}, \dfrac{\partial J}{\partial c}, \dfrac{\partial J}{\partial d}, \dfrac{\partial J}{\partial e} \rangle \\ \dfrac{\partial J}{\partial a} = \dfrac{T \cdot KS}{n} \sum\limits_{i=1}^{n} (h_\theta(x^{(i)}) - Y^{(i)}) x^{(i)} \\ \dfrac{\partial J}{\partial b} = \dfrac{V \cdot KS}{n} \sum\limits_{i=1}^{n} (h_\theta(x^{(i)}) - Y^{(i)}) x^{(i)} \\ \dfrac{\partial J}{\partial c} = \dfrac{h \cdot KS}{n} \sum\limits_{i=1}^{n} (h_\theta(x^{(i)}) - Y^{(i)}) x^{(i)} \\ \dfrac{\partial J}{\partial d} = \dfrac{KS}{n} \sum\limits_{i=1}^{n} (h_\theta(x^{(i)}) - Y^{(i)}) x^{(i)} \\ \dfrac{\partial J}{\partial e} = \dfrac{R_0 \cos e_i}{n} \sum\limits_{i=1}^{n} (h_\theta(x^{(i)}) - Y^{(i)}) x^{(i)} \end{cases} \tag{13}$$

The gradient is given as a vector whose direction indicates the direction in which the function rises fastest at the given vertex. Therefore, in order to find the local optimal point, the negative gradient direction is chosen as the optimal direction. Then:

$$\theta_1 = \theta_0 - \alpha \bigtriangledown J(\theta) \tag{14}$$

α is the learning rate, which determines the speed of gradient descent. The initial value is 0.1. The updated formula is as Eq. (15).

$$\alpha = \begin{cases} \alpha_{i+1} = \alpha_i \cdot 1.05, (J(\theta_i) < J(\theta_{i-1})) \\ \alpha_{i+1} = \alpha_i \cdot 0.5, (J(\theta_i) > J(\theta_{i-1})) \end{cases} \tag{15}$$

If the value J of the cost function of the first order is less than that of the cost function of the first order, the learning rate will increase by 5%. On the contrary, it changes to 50% of the original value and resets the value of the iteration variable of the first time. Following the above principles, the training data values are optimized by regression.

The experimental site is located in Hongqi Forest Farm, Hegang City, Heilongjiang Province, 130°E east longitude and 47°N north latitude, late November. On the day of ignition, the average temperature was 11°C, the Buffalo wind class was 2, and the humidity was 71%. The burning site was meadow, so the combustible index Ks was 1.8. The optimization results were as Fig. 8:

In Figure 7, the red dot is the experimental measured point, and the blue line is the fitting curve. It can be seen that the trend of forest and area spread can be basically fitted with good optimization results. The parameters of the optimized formula are as Tab. 1:

By using the spread formula after regression and Wang Zhengfei's spread model before revision, the last

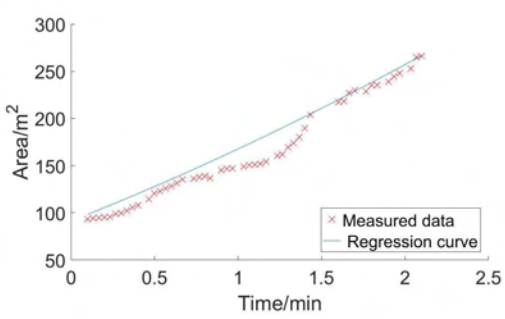

Figure 8: The results of gradient descent optimization

Table 1: Comparison of optimized(2) and unoptimized(1) parameters

Index	a	b	c	d	e
(1)	0.4256	0.4257	−1.412	−1.107	1.91
(2)	0.03	0.05	−0.01	−0.3	1.8

14 time points of the experimental data were predicted, and the evaluation and analysis of the regression model were compared with the measured values. As shown in Fig. 9, the "×" symbol represents the data of the measured value, the "○" symbol represents the predicted value after regression, and the "◇" symbol represents the predicted value of the original parameter. It is obvious that the calculated results of the model without modification are quite different from the actual values, and the predicted values of the model after modification are in good agreement with the measured values. Based on this result, the model will be evaluated from three aspects.

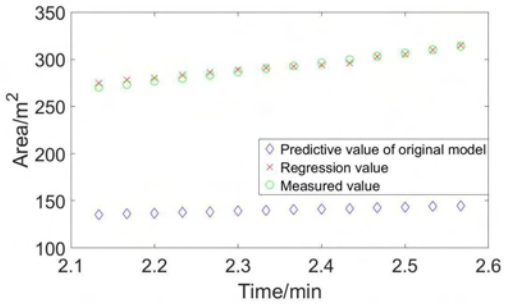

Figure 9: Comparison of regression value, measured value and predicted value of unmodified model

4.2 Model assessment

4.2.1 The goodness of fit-R^2

In regression prediction, the fitted line is only an approximate curve, and it is impossible to include all points. Therefore, in order to evaluate the goodness of fit, the goodness of fit-R^2 (Zendehdel, 2018) is used to judge the goodness of fit of regression equation.

$$R^2 = \frac{SSR}{SST} = \frac{SSR}{SSE + SSR} \tag{16}$$

In the above Eq. (16), SSR is the sum of regression squares, SSE is the sum of residual square, and the sum of the two SST is the sum of total deviation squares.

The sum of regression squares is shown in Eq. (17). The change of the difference between regression value and mean value is caused by the change of time of independent variable, which reflects the change of area caused by the linear relationship between area and time in the total deviation, and can be explained by the regression line.

$$SSR = \sum_{i=1}^{n} (\widehat{Y}_i - \bar{Y})^2 = (\widehat{Y}_1 - \bar{Y})^2 + \ldots + (\widehat{Y}_n - \bar{Y})^2 \tag{17}$$

From fourteen experimental data, the mean value of measured value $\bar{Y}$=292.68 m^2 can be obtained, and the difference between the regression value of corresponding points and the mean value of measured value is as Tab. 2.

Table 2: The Difference between the Mean of Regression Value and the Measured Value

$Time(min)$	$\widehat{Y}_i - \bar{Y}$	$Time(min)$	$\widehat{Y}_i - \bar{Y}$
2.13	−22.71	2.36	0.41
2.16	−19.45	2.40	3.78
2.20	−16.17	2.43	7.15
2.23	−12.88	2.46	10.54
2.26	−9.58	2.50	13.95
2.30	−6.26	2.53	17.37
2.33	−2.92	2.56	20.80

From Tab. 2 can be obtained:$SSR = 2568\ m^2$.

The sum of squares of residuals is shown in Eq. (18). This difference represent the effect of factors other than the linear effect of time on area, which cannot be explained by regression lines.

$$SSE = \sum_{i=1}^{n} (\widehat{Y}_i - Y_i)^2 = (\widehat{Y}_1 - Y_i)^2 + \ldots + (\widehat{Y}_n - Y_i)^2 \tag{18}$$

Table 3: The difference between the regression value and the measured value

$Time(min)$	$\widehat{Y}_i - \bar{Y}$	$Time(min)$	$\widehat{Y}_i - \bar{Y}$
2.13	−4.77	2.36	0.51
2.16	−4.81	2.40	2.30
2.20	−3.66	2.43	3.8
2.23	−3.17	2.46	0.52
2.26	−2.42	2.50	1.10
2.30	−1.28	2.53	1.47
2.33	−0.51	2.56	−1.42

From the experiment data, the difference between the regression value and the measured value can be obtained as Tab. 3:

According to the table above, the sum of regression squares can be obtained:$SSE = 110.82\ m^2$.

Two different differences distributions are shown in Fig. 10. The green point is the difference between the regression value corresponding to a certain time point and the mean value of the measured value ($\widehat{Y}_i - \bar{Y}$), it can be seen that the difference varies with the time of independent variable x. The red dot is the difference between the regression value corresponding to a certain time point and the measured value ($\widehat{Y}_i - Y_i$), it can be seen that the distribution is not only affected by the independent variable x time, but also irregular.

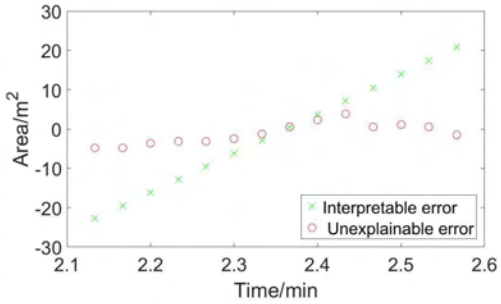

Figure 10: Two different differential distributions

The sum of squares of total deviations is the sum of the two, which reflects the general fluctuation of the values of dependent variables. By dividing SSR and SST, we can get the proportion of errors in the total fluctuation. This proportion is between 0 and 1, the better the fitting degree of the regression equation is. According to the above, the goodness of fit can be obtained as Eq. (19).

$$R^2 = \frac{SSR}{SST} = \frac{SSR}{SSE + SSR} = 0.9586 \tag{19}$$

Finally, the goodness of fit is 0.9586, which should be a good value, indicating that the regression equation

fits 14 test values very well. This is also related to the specific ignition experiment on that day. When the fire started to spread, it was affected by many external factors. After that, when the fire increased, it gradually spread in accordance with a basically fixed trend.

The accuracy of the model can be expressed by $RMSE$. The root mean square error, also known as standard error, is the square root of the mean of the deviation between the regression value and the measured value. Standard error is very sensitive to a group of large or small errors in measurement so standard error can well reflect the precision of measurement. The square sum of the difference between the regression value and the measured value is the SSE mentioned above, so the root mean square error can be obtained as Eq. (20).

$$RMSE = \sqrt{\frac{1}{N}\sum_{i=1}^{n}(\widehat{Y}_i - Y_i)^2} = \sqrt{\frac{SSE}{N}} \tag{20}$$

Among the Eq. (20), SSE is obtained from the above, N is the number of experimental data, and there are fourteen test data sets, which can be obtained: $RMSE = 2.8136\ m^2$.

The result is within the acceptable range of error relative to the actual area of the fire field.

4.2.2 Residual Analysis

The residual error is the difference between the regression value of the dependent variable time and the measure value, represented by ei. The residual is regarded as the observed value of the error. Residual analysis (Jia et al., 2018) can be used to examine the rationality of model assumptions and the reliability of data. The commonly used residuals are ordinary residuals, internalized residuals and externalized residual. This paper chooses to analyze the internalized residuals (Li et al., 2008). The internalized residuals also become standardized residuals. If the residual ei obeys the normal distribution $N(0, ei^2)$, and if the standardized residual ei^* is obtained by standardizing ei, then the ei^* will obey the normal distribution $N(0, 1)$. If the assumption that the error term obeys normal distribution holds, then the distribution of standardized residuals obeys normal distribution, then about 95% of standardized residuals are between -2 and 2. As shown in Fig. 11.

By comparing the normalized residual distribution before and after the revision, the optimization degree of the model can be seen intuitively. Standardized residuals are represented by Z_{ei}, the corresponding standardized residuals of observed values as Eq. (21).

$$Z_{ei} = \frac{ei}{S_e} = \frac{\widehat{Y}_i - Y_i}{S_e} \tag{21}$$

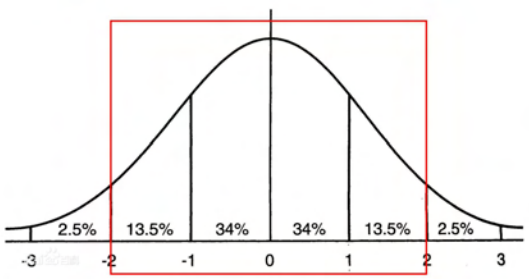

Figure 11: Normal Distribution of Standardized Residual

S_e is the standard deviation estimate of the residuals. The standard deviation formula is as Eq. (22).

$$S_e = \sqrt{\frac{1}{N}\sum_{i=1}^{N}(e_i - \bar{e})^2} \tag{22}$$

In order to better reflect the difference between before and after optimization, the standardized residuals can be obtained by using the parameters of Wang Zhengfei's model before and after modification, as shown in Fig. 12.

From Fig. 12a, it can be seen that the standardized residuals generated by the optimized model are between -2 and 2, which proves that the error of regression equation is within acceptable range. However, the standard deviation of the unmodified spreading velocity model in Fig. 12b is larger and less than 0, which indicates that the unmodified Wang Zhengfei's model does not predict the trend of forest fire spread sufficiently and underestimates the trend of forest fire spread. The corrected model based on the measured data in this paper can achieve good prediction results.

5 CONCLUSION

Forest fire spread is a research field with changeable conditions and complex factors, so no model can absolutely apply to all cases of forest fire spread. In this paper, ZED camera is used to collect real-time data and modify the parameters of forest fire spread model in order to better predict the spread of forest fire.

On the basis of previous studies, this paper presents a new method for monitoring the spread trend of forest fire. Using ZED camera to shoot spot burning video, the spread speed and area of fire can be obtained by processing video image. The parameters of the new model, which is established by Wang Zhengfei model and Huygens' theory, are corrected by using the collected data. Finally, the goodness of fit, root mean square error and residual diagram are evaluated and analyzed. The goodness of fit reached 0.9586, indicating

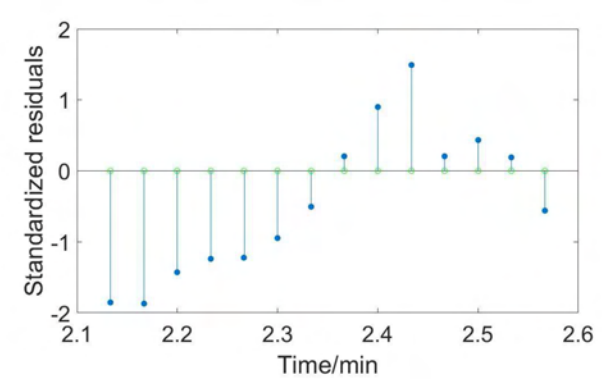

(a) Standardized residuals after optimization

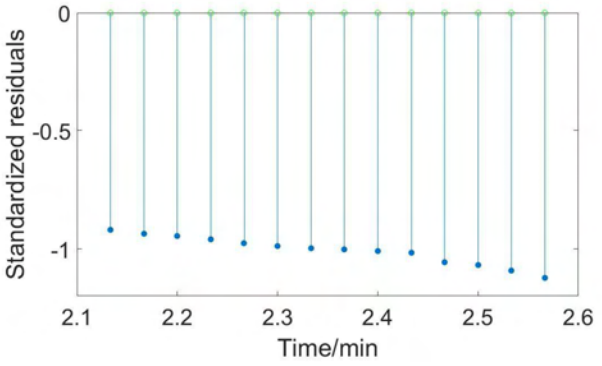

(b) Standardized residuals before optimization

Figure 12: Standardized residuals

that the model could well fit the development trend of experimental data and accurately predict the development rate of forest fire spread. The root-mean-square error is 2.8136 m^2, which reflects that the error of the model is controlled in a small range and can be accepted by a wide range of point burning experiments. The prediction effect of modified model and unmodified model is compared by residual diagram, which proves that the modified extended model has higher prediction accuracy.In addition, ZED camera is very effective to collect data and save a lot of manpower and material resources. The experimental results also prove the feasibility of this method.Moreover, the test method by using ZED camera to collect data is very efficient, which saves a lot of manpower and materials. The results also prove the feasibility of this method.

Limited by the previous experimental conditions, the detection of some variables such as wind speed and humidity in this experiment is not very comprehensive, and the data can not be collected in real time like ZED video. This is still much space for improvement of the model results. In the future research, I hope that I can control variables more deeply and better reflect the impact of relevant variables from the model. For forest fire detection, it is also hoped that there will be better management and control of fire prevention measures, better prediction of fire, simulation of fire and eventual extinguishment, and more scientific methods for forest fire prevention research.

Acknowledgement

Thanks are due the meticulous comments made by several experts during the peer-review process to make this article more complete. Thanks are due to the Key Laboratory of Sustainable Forest Ecosystem Management-Ministry of Education for its strong support for this project.

Funding for this study has been provided by the The National Key Research and Development Program of China (2018YFD0600205); Fundamental Research Funds for the Central Universities (Grant No.2572019CP20, 2572019CP10).

References

Al-Tairi, Z. H., Rahmat, R. W. O., Saripan, M. I., & Sulaiman, P. S. 2014. Skin Segmentation Using YUV and RGB Color Spaces. JIPS, 10(2), 283–299. DOI:10.3745/JIPS.02.0002.

Anderson, H. E. 1983. Predicting wind-driven wind land fire size and shape (Vol. 305). US Department of Agriculture, Forest Service, Intermountain Forest and Range Experiment Station.

Chen, Z., Sun, T., Zhang, L., & Qin, Q. 2012. Forest fire spread fast model based on 3D cellular automaton in spatially heterogeneous area. Journal of Beijing Forestry University, 34(1), 86–91. DOI:10.13332/j.1000-1522.2012.01.014.

Ervilha, A. R., Pereira, J. M. C., & Pereira, J. C. F. 2017. On the parametric uncertainty quantification of the Rothermel's rate of spread model. Applied Mathematical Modelling, 41, 37–53. DOI:10.1016/j.apm.2016.06.026.

Han, X. F., Jin, J. S., Wang, M. J., Jiang, W., Gao, L., & Xiao, L. P. 2017. Video fire detection based on gaussian mixture model and multi-color features. Signal, Image and Video Processing, 11(8), 1419–1425. DOI:10.1007/s11760-017-1102-y.

Milios, E., Kitikidou, K., Pipinis, E., Stampoulidis, A., & Gotsi, M. 2018. ESTIMATING TREE BOLE HEIGHT WITH BAYESIAN ANALYSIS. Mathematical and Computational Forestry & Natural-Resource Sciences (MCFNS), 10(2), 58-67(10). Re-

trieved from http://mcfns.net/index.php/Journal/-article/view/10.12

Jia, R. Y., & Li, Y. G. (2018). K-Means Algorithm of Clustering Number and Centers Self-Determination. Computer Engineering and Applications, 54, 152–158. DOI:10.3778/j.issn.1002-8331.1610-0342.

Li Q., Zhiping, L.V. 2008. Fuzzy Adaptive Kalman Filtering Algorithm Based on the Statistics of t Distribution. Acta Geodetica et Cartographica Sinica, 37(4):428–432. DOI:10.3321/j.issn:1001-1595.2008.04.005.

Liu Xiaozhi, Didi, Q., & Chi, B. 2017. Camera Calibration Method Based on Distortion Separation. Journal of Northeastern University. Natural Science, 38(5):620–624. DOI:10.3969/j.issn.1005-3026.2017.05.003.

Richards, G. D. 1993. The properties of elliptical wildfire growth for time dependent fuel and meteorological conditions. Combustion science and technology, 95(1-6), 357–383.

Tang, L., Hanghui, M., Chongcheng, & C., Hongyu, H. 2015. Three-dimensional visual simulation of forest fire spread based on FARSITE. Journal of Natural Disasters, 24(2):221–227. DOI:10.13577/j.jnd.2015.0228.

Technikova, L., & Tunak, M. 2016. Comparison of two different principles of 3D fabric surface reconstruction. Fibres & Textiles in Eastern Europe 24(5):38–43. DOI:10.5604/12303666.1215525.

Xiao-hong, W. A. N. G., Ji-li, Z., & Sen, J. 2013. Research progress of forest fire spreading simulation. Journal of Central South University of Forestry and Technology, 33(10), 69–77. DOI:10.14067/j.cnki.1673-923x.2013.10.014.

Wang, Y., Wang, X., & Yin, L. 2019. Estimation of extrinsic parameters for dynamic binocular stereo vision using unknown-sized rectangle images. Review of Scientific Instruments, 90(6):65–108. DOI:10.1063/1.5086352.

Wu, X., Yan, Y. Y., Du, J., Gao, S. B., & Liu, Y. A. 2015. Fire detection based on fusion of multiple features. CAAI Transactions on Intelligent Systems, 10(2):240–247. DOI:10.3969/j.issn.1673-4785.201406022.

Fulong, Y. 2016. Study on simulation of three dimensional simulation of forest fire spread based on cellular automaton. Computer Engineering and Application, 52(19), 37–41. DOI:10.3778/j.issn.1002-8331.1508-0093

Zendehdel, J., Rezaei, M., Akbari, M. G., Zarei, R., & Noughabi, H. A. 2018. Testing exponentiality for imprecise data and its application. Soft Computing, 22(10), 3301–3312. DOI:10.1007/s00500-017-2566-y.

Willson, D., Monleon, V., & Weiskittel, A. 2019. Quantification and Incorporation of Uncertainty in Forest Growth and Yield Projections Using A Bayesian Probabilistic Framework: A Demonstration for Plantation Coastal Douglas-fir in the Pacific Northwest, USA. Mathematical and Computational Forestry & Natural-Resource Sciences (MCFNS), 11(2), 264-285(22). Retrieved from http://mcfns.net/-index.php/Journal/article/view/11.3.

Zhao, M., Zhang, Z., Cheng, C., & Hao, X. 2018. A method for straight image distortion correction using a single image. Journal of Wuhan University. Information Science Edition, 43(1), 60–66. DOI:10.13203/j.whugis20150445.